Microwave synthesis and magnetic properties of bismuth ferrite nanopowder doped with cobalt*

E. V. Tomina,[a]★ N. S. Perov,[b] I. Ya Mittova,[a] Yu. A. Alekhina,[b] O. V. Stekleneva,[a] and N. A. Kurkin[a]

[a]*Voronezh State University,*
1 Universitetskaya pl., 394006 Voronezh, Russian Federation.
E-mail: tomina-e-v@yandex.ru
[b]*Lomonosov Moscow State University, Department of Physics,*
Build. 2, 1 Leninskie Gory, 119991 Moscow, Russian Federation

A technique for the synthesis of bismuth orthoferrite nanopowder doped with cobalt ions activated using microwave radiation is proposed. Exposure to microwave radiation followed by ultrasonic treatment of the synthesized $BiFeO_3$ samples using sodium hydroxide as a precipitant makes it possible to obtain spherical $BiCo_xFe_{1-x}O_3$ particles with a narrow particle-size distribution in the range of 35—60 nm. Bismuth ferrite doped with cobalt ions has a considerably higher magnetization and magnetic susceptibility than an undoped $BiFeO_3$.

Key words: multiferroics, nanopowders, bismuth orthoferrite, doping.

Bismuth ferrite $BiFeO_3$, a complex oxide with a perovskite-like structure, is a promising multiferroic which can be used in various new electronic devices. High temperatures of magnetic (Neel temperature T_N ~643 K) and ferroelectric ordering (Curie temperature T_C ~1083 K) indicate that the magnetoelectric effect can be expected to manifest itself at high operating temperatures, provided that the spatially modulated spin structure is suppressed.

Magnetoelectric materials are necessary for the development of fundamentally new spintronic devices, including those used for computer memory, as well as ultra-sensitive sensors of constant and alternating magnetic fields for various purposes (medicine, navigation, instrumentation), phase shifters and switching elements for optics, devices for the conversion of electromagnetic field energy, microwave equipment precision devices.[1—6] Various methods are used for the suppression of the spin cycloid: the application of a strong magnetic field, the replacement of bismuth ions with ions of rare earth elements or iron ions with 3d-metals, the manufacture of $BiFeO_3$ thin films, *etc.*[7—12]

Doping of bismuth ferrite with d-metals,[13,14] which have their own magnetic moments, improves the magnetic and ferroelectric properties of $BiFeO_3$, extends the interval of formation of continuous solid solutions, and increases the thermal stability of $BiFeO_3$.

The synthesis of $BiFeO_3$ is fraught with difficulties primarily related to the need to obtain the product as a pure phase. Based on the works,[15—21] it was suggested that microwave synthesis can be used to prepare individual phases of monodisperse nanoparticles with reproducible compositions and sizes at a low temperature and with a short process duration (Table 1).

Table 1. Qualitative comparison of advantages offered by bismuth ferrite synthesis methods

Synthesis method	Possibility of doping	Particle size/nm	Synthesis temperature/°C	Synthesis duration	Simplicity	Content of impurities
Ceramic method[15,16]	Yes	~200	>800	Hours (sometimes days)	–	Considerable
Pechini method[17]	Yes	20—25	~100—350	Hours (sometimes days)	–	Considerable
Hydrothermal synthesis[18]	Yes	12—27	<500	Hours	–	~7%
Microwave synthesis[19,20]	Yes	35—60	~100	Hours	+	Negligible
Aerosol spray pyrolysis method[22]	Yes	33—57	~760	Hours	+	Negligible

* Based on the materials of the XXI Mendeleev Congress on General and Applied Chemistry (September 9—13, 2019, St. Petersburg, Russia).

Published in Russian in *Izvestiya Akademii Nauk. Seriya Khimicheskaya,* No. 5, pp. 0941—0946, May, 2020.

The goal of this work is to carry out a synthesis of $BiFeO_3$ and $BiCo_xFe_{1-x}O_3$ nanopowders activated by microwave radiation and to determine the effect of cobalt doping of bismuth ferrite on the magnetic properties of the samples.

Experimental

Crystalline hydrates $Fe(NO_3)_3 \cdot 9H_2O$ (analytical grade, TU 6-09-02-553-96) and $Bi(NO_3)_3 \cdot 5H_2O$ (analytical grade, CAS 10035-06-0), cobalt nitrate $Co(NO_3)_2 \cdot 6H_2O$ (analytical grade, GOST 4528-78), sodium hydroxide NaOH (analytical grade, GOST 432877) were used as precursors. Bismuth ferrite was deposited from a solution of starting nitrates under microwave radiation from a source with $P_{max} = 800$ W (operating frequency 2450 MHz).[10] In the synthesis of cobalt doped bismuth ferrite, the concentrations of cobalt and iron ions were calculated using the stoichiometric ratio: $Bi^{3+} : Co^{2+} : Fe^{3+} = 1 : x : (1 - x)$, where $x = 0.05$, 0.10, 0.15 is the targeted degree of doping.

The calculated amounts of iron nitrate, bismuth nitrate, and cobalt nitrate crystalline hydrates were dissolved in distilled water, and a 20% NaOH solution was added to the resulting solution. The resulting solution was exposed to microwave radiation with $P_{max} = 700$ W for 10 min, followed by exposure to ultrasound (VU-09-Ya-FP-02) for 15 min to activate the synthesis of bismuth ferrite. After cooling to ~20 °C, the bismuth ferrite precipitate was isolated from the solution by centrifugation, dried in air, and calcined in a muffle furnace (SNOL 8.2/1100) at 500 °C for 2 h.

To study the phase composition of the sample and the sizes of crystallites, powder X-ray diffraction (DRON-3 X-ray diffractometer with a Mo anode ($\lambda = 0.71075$ nm)) was used. X-ray diffractograms were recorded from 6 to 40° (2θ) with a step of 0.05°. The size of CSR (coherent scattering regions) was calculated by the Scherrer equation from the standard peak broadening.

The synthesized $BiFeO_3$ and $BiCo_xFe_{1-x}O_3$ samples were studied on a Vertex-70 IR Fourier spectrometer (spectral resolution 0.5 cm^{-1}, spectral range 400—4000 cm^{-1}), transmission spectra were recorded.

Energy dispersive spectra were recorded on a JEOL-6510LV scanning electron microscope with an energy dispersive microanalysis system (Bruker).

The size and morphology of the particles of the synthesized powders was determined using transmission electron microscopy (TEM, Carl Zeiss Libra-120 transmission electron microscope).

Magnetic properties were measured using a model 7407 LakeShore magnetometer in fields of up to 1591549.43 A m^{-1} (20 kOe) in a nitrogen cryostat. A sample with a weight of 15—30 mg was used, which was packaged into a polyethylene phthalate micropack. Sample sizes did not exceed 4×5×0.5 mm. An in-plane external field was applied to the sample to minimize the demagnetizing effect.

Results and Discussion

Powder X-ray diffraction results (Fig. 1) indicate that the synthesized samples are bismuth orthoferrite $BiFeO_3$ (card number 73-0548). Single reflections of $Bi_{25}FeO_{39}$ and $Bi_2Fe_4O_9$ phases are also present (card numbers 46-0416, 72-1832).[23]

A comparison of the diffraction patterns of $BiCo_{0.05}Fe_{0.95}O_3$, $BiCo_{0.10}Fe_{0.90}O_3$, and $BiCo_{0.15}Fe_{0.85}O_3$ samples (see Fig. 1) exhibits a shift of the reflections relative to those of the undoped sample toward larger 2θ angles, which indicates a contraction of the crystal lattice due to the substitution of the ion with a larger radius with an ion with a smaller radius.[24] In consideration of the charge state of the dopant,[24] it is appropriate to take into account a rapid change of the oxidation state of cobalt from +2 to

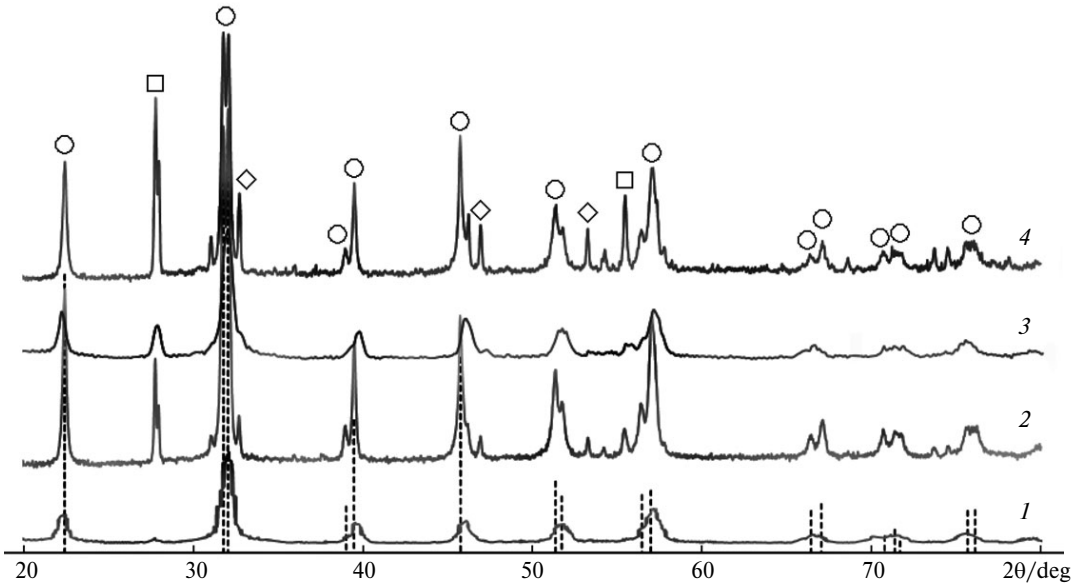

Fig. 1. X-ray diffraction patterns of $BiFeO_3$ (*1*), $BiCo_{0.05}Fe_{0.95}O_3$ (*2*), $BiCo_{0.10}Fe_{0.90}O_3$ (*3*), $BiCo_{0.15}Fe_{0.85}O_3$ (*4*). The symbols "○", "□", and "◊" indicate $BiFeO_3$, $Bi_{25}FeO_{39}$, and $Bi_2Fe_4O_9$ reflections, respectively.

+3 that may initiate the oxidative thermolysis of cobalt nitrate when the starting mixture undergoes a microwave heating. This in turn can lead to the formation of Co_3O_4 as evidenced by our experimental results.[25] Therefore, we can assume that cobalt ions are mainly in the state Co^{3+} during the synthesis of doped $BiFeO_3$ samples. Cobalt ions can be incorporated into the ferrite lattice in sites previously occupied by iron cations due to the similarity of their atomic characteristics and crystallochemical parameters. Apparently, this process is what is observed when cobalt is introduced. This suggestion is supported by crystallochemical results indicating either identical (0.055 nm)[26] or very similar[26] Co^{3+} (0.061 nm) and Fe^{3+} (0.064 nm) radii. The possibility of isomorphous substitution of Fe^{3+} and Co^{3+} is indirectly confirmed by the shift of the strongest reflection in the diffraction patterns of $BiFeO_3$ toward a larger 2θ angles with an increasing degree of doping with cobalt. The Co^{2+} cations have a radius of 0.074 nm, which is larger than the ionic radius of Fe^{3+}, and, in principle, can occupy the position of Bi^{3+} (ionic radius equal to 0.120 nm).[27] In reality, the incorporation of cobalt into the bismuth ferrite lattice replacing iron ions is confirmed by the contraction of the crystal lattice (Table 2).

The energy dispersive spectra of the synthesized $BiCo_xFe_{1-x}O_3$ samples include not only Bi, Fe, and O signals, but also Co signals (Fig. 2), which once again confirms the inclusion of cobalt into the $BiFeO_3$ lattice. Cobalt signals in the spectra of the synthesized samples grow in intensity with an increasing degree of doping of bismuth ferrite.

The calculation of CSR for the synthesized ferrite samples using the Scherrer formula showed that the average particle sizes of $BiFeO_3$, $BiCo_{0.05}Fe_{0.95}O_3$, $BiCo_{0.10}Fe_{0.90}O_3$, and $BiCo_{0.15}Fe_{0.85}O_3$ are in the range of 17—67 nm (Table 3), and the particle diameter is much smaller for doped ferrite compared to undoped $BiFeO_3$.

According to TEM (Fig. 3, *a*), $BiFeO_3$ particles are predominantly spherical and agglomerated, particle sizes are in the range of 35—60 nm. The sizes of most particles are in the range of 35—55 nm.

In the case of $BiCo_{0.10}Fe_{0.90}O_3$, the particles have a spherical shape (Fig. 3, *b*—*e*), the predominant particle size is 1—20 nm (Fig. 4). Some agglomerates with sizes of up to 60 nm are observed (see Fig. 3, *a*).

Table 2. Lattice parameters of the synthesized samples

Sample	*a*	*c*	*V*/Å^3
	Å		
Standard, $BiFeO_3$ (card 73-0548)	5.58	13.9	374.81
$BiCo_{0.05}Fe_{0.95}O_3$	5.5722±0.05	13.8570±0.13	372.61±0.37
$BiCo_{0.15}Fe_{0.85}O_3$	5.5707±0.05	13.8529±0.13	372.49±0.37

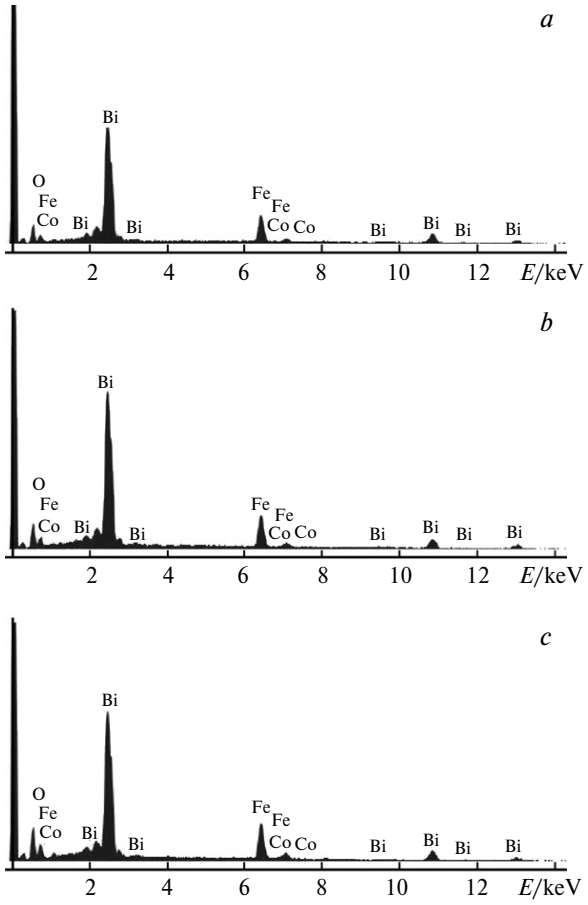

Fig. 2. Energy dispersive spectra of $BiCo_{0.05}Fe_{0.95}O_3$ (*a*), $BiCo_{0.10}Fe_{0.90}O_3$ (*b*), $BiCo_{0.15}Fe_{0.85}O_3$ (*c*).

In general, TEM results confirm the calculations of CSR based on powder X-ray diffraction results. Some overestimation of the latter in comparison with TEM results is related with the specific features of the methods used. The determination of the average size of CSR with the Scherrer formula using the width of the diffraction maximum can lead to errors caused by the following reasons. First, mathematical models used to analyze the profiles of X-ray lines when determining the distribution

Table 3. Size of the CSR* (powder X-ray diffraction results) of $BiCo_xFe_{1-x}O_3$ particles with targeted cobalt content $x = 0$—0.15

Sample	D_1	D_2	D_3	D_{av}
	nm			
$BiFeO_3$	66±3	54±2	80±4	67±3
$BiFeO_3$—Co(5%)	23±2	19±1	20±2	21±2
$BiFeO_3$—Co(10%)	15±1	13±1	25±2	17±1
$BiFeO_3$—Co(15%)	48±3	21±1	47±2	39±2

* *D* is nanoparticle diameter.

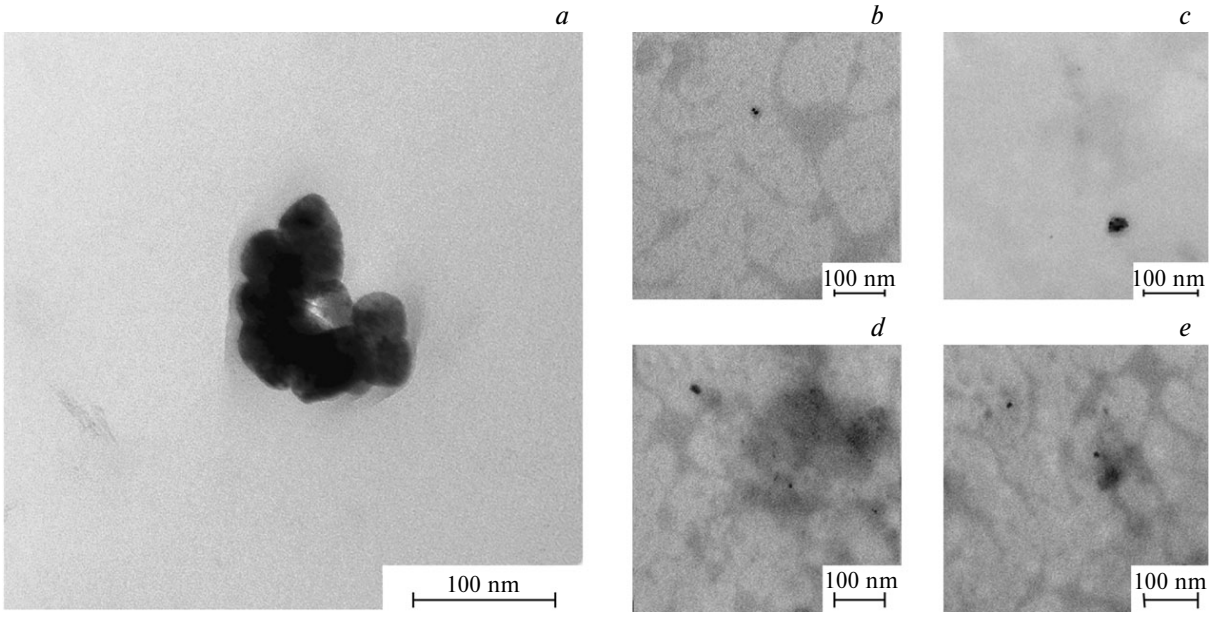

Fig. 3. TEM images in the gelatin layer of $BiFeO_3$ (*a*) and various $BiCo_{0.10}Fe_{0.90}O_3$ particles (*b*—*e*).

of particle sizes are different. Second, the broadening of diffraction maxima can be affected by various factors, in particular, the presence of defects and microstrains. In addition, the diffraction method characterizes the bulk structure and is therefore used to determine particle size which is averaged over the entire volume, in contrast to electron microscopy, which is a direct local visual method for estimating particles size.

The field dependence of magnetization of undoped $BiFeO_3$ is nearly linear both at a temperature of 300 K (Fig. 5, *a*) and at a temperature which is decreased to 100 K (Fig. 5, *b*).

The specific magnetization of $BiFeO_3$ reaches 11.3 A m^2 kg^{-1} at a temperature of 300 K in a field of 16 kOe (1273239 A m^{-1}), and with a temperature decreasing to 100 K it increases to 18.2 A m^2 kg^{-1} (almost half as much again) (Table 4).

The introduction of a dopant changes the magnetic structure of bismuth ferrite, which is observed on the magnetization curves of the samples. The field dependences of the magnetization of $BiCo_{0.1}Fe_{0.90}O_3$ and $BiCo_{0.15}Fe_{0.85}O_3$ samples have distinctive bends at a magnetic field of ~2500 Oe (198943 A m^{-1}). The shape of the hysteresis loop indicates that magnetic saturation is not achieved in a field of up to 16 kOe (1273239 A m^{-1}). The

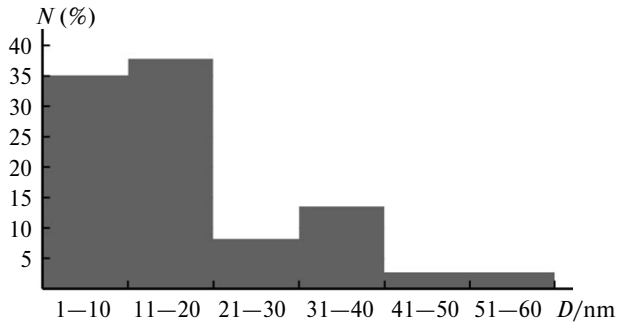

Fig. 4. Histogram of the particles-size distribution for $BiCo_{0.10}Fe_{0.90}O_3$ according to TEM; *N* is the fraction of particles.

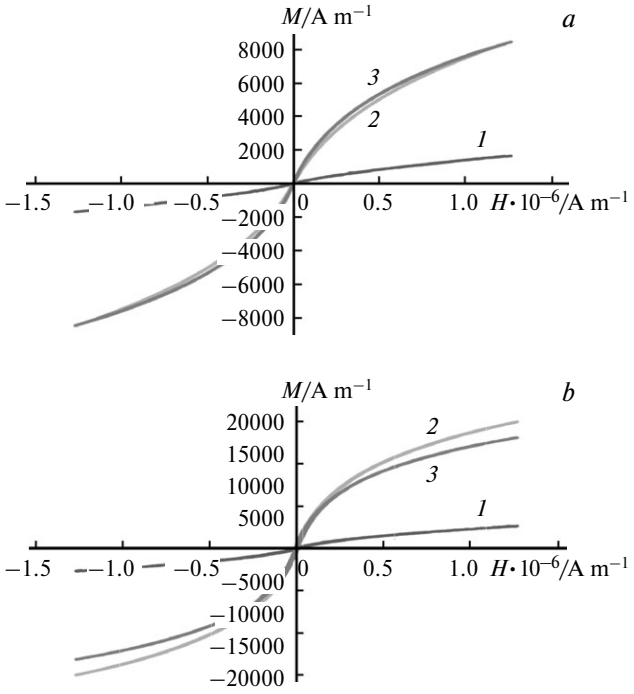

Fig. 5. Field dependence of the magnetization (*M*) of $BiFeO_3$ (*1*), $BiCo_{0.10}Fe_{0.90}O_3$ (*2*), and $BiCo_{0.15}Fe_{0.85}O_3$ (*3*) (calcined at 500 °C, 2 h) samples, measured at 300 (*a*) and 100 K (*b*); *H* is the magnetic field.

Table 4. Magnetic characteristics of $BiFeO_3$, $BiCo_{0.10}Fe_{0.90}O_3$, and $BiCo_{0.15}Fe_{0.85}O_3$ samples, measured at temperatures of 300 and 100 K

Sample	T/K	Specific magnetization	Residual magnetization	Magnetic susceptibility/kg^{-1}
		A m^2 kg^{-1}		
$BiFeO_3$	300	11.3	0.1	4230
	100	18.2	0.6	6785
$BiCo_{0.10}Fe_{0.90}O_3$	300	39.5	0.2	8414
	100	61.2	1.5	13050
$BiCo_{0.15}Fe_{0.85}O_3$	300	33.2	0.3	8420
	100	58.6	2.3	14870

specific magnetization of $BiCo_{0.1}Fe_{0.90}O_3$ and $BiCo_{0.15}Fe_{0.85}O_3$ in a field of 16 kOe (1273239 A m^{-1}) at a temperature of 100 K is 61.2 and 58.6 A m^2 kg^{-1} (see Table 4), respectively. The magnetization of both samples decreases with a temperature increasing to 300 K (39.5 A m^2 kg^{-1} for $BiCo_{0.1}Fe_{0.90}O_3$ and 33.2 A m^2 kg^{-1} for $BiCo_{0.15}Fe_{0.85}O_3$), but remains much higher than the magnetization of undoped bismuth ferrite (see Table 4).

In general, the magnetization of both undoped bismuth ferrite and $BiCo_{0.1}Fe_{0.90}O_3$, $BiCo_{0.15}Fe_{0.85}O_3$ samples steadily decreases with increasing temperature (Fig. 6). The specific magnetization of $BiCo_{0.1}Fe_{0.90}O_3$ is slightly higher than that of $BiCo_{0.15}Fe_{0.85}O_3$ at all temperatures, despite higher dopant content in the latter, which is probably due to the presence of $Bi_{25}FeO_{40}$ impurities in the sample (powder X-ray diffraction results), whereas in the diffraction pattern of $BiCo_{0.1}Fe_{0.90}O_3$ the $Bi_{25}FeO_{40}$ maxima are much weaker (see Fig. 1). Nevertheless, the ferromagnetic behavior of the samples observed at room temperature reflects the properties of the principal $BiCo_{0.1}Fe_{0.9}O_3$ and $BiCo_{0.15}Fe_{0.85}O_3$ phases only, because the $Bi_{25}FeO_{39}$ impurity phase, traces of which were detected using powder X-ray diffraction, is not ferromagnetic at room temperature. The $Bi_2Fe_4O_9$ impurity phase is antiferromagnetic until a temperature of 258 °C is reached.[28]

The stability of the magnetic structure of a substance is related to the persistence of the crystal structure, and the nature of the exchange interactions is strongly dependent on the parameters of the crystal lattice. The change of the magnetic properties of doped samples can be caused by the distortions of crystallographic parameters because of the difference in the ionic radii of cobalt and iron. The distortions of the starting matrix ($BiFeO_3$), caused by the size factor, leads to changes in bond angles and bond lengths for Fe—O—Fe, and, consequently, the strength of the exchange interaction. Doping of bismuth ferrite with cobalt ions leads to the formation of Fe—Co—Fe and Fe—O—Co—Fe configurations, which tend toward ferromagnetic ordering.[29] A possible approach for increasing magnetization is an increase of the spin-orbit coupling constant for cobalt atoms, which increases the rotation angle of magnetic sublattices in the antiferromagnet.[30] Bismuth ferrite doped with cobalt ions may be a promising catalyst for the oxidination of semiconductors, on the surface of which dielectric and semiconductor films with thicknesses in the nanoscale range rapidly form. Bismuth compounds, as we have shown earlier,[31] are effective stimulants of thermoxidation of semiconductors, iron can perform a catalytic function in these processes, and cobalt can take part in both.[32] Using nanoscale nanostructured yttrium ferrite films deposited on a silicon surface as an example, we have established that magnetic properties of these objects persist in the film state,[21] which makes it possible to use the magnetic field to control heterogeneous catalytic processes in new systems that operate with a thin-film catalyst, reagents, and products.

In conclusion, a technique has been developed for the synthesis of $BiFeO_3$ and $BiCo_xFe_{1-x}O_3$ nanopowders activated by microwave radiation, which allows the formation of samples with high chemical homogeneity. The synthesized powders have particles of predominantly spherical shape and are up to 100 nm in size with most particles having sizes in the range of 35—55 nm for $BiFeO_3$ and 10—15 nm for $BiCo_{0.1}Fe_{0.90}O_3$. Doping of $BiFeO_3$ with cobalt leads to a considerable increase of the specific

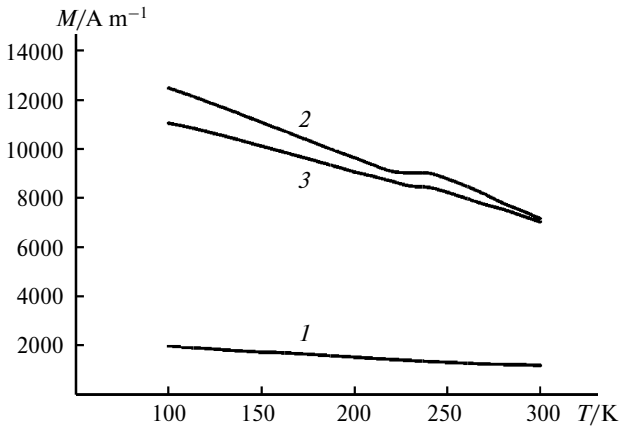

Fig. 6. Temperature dependence of the magnetization of $BiFeO_3$ (*1*), $BiCo_{0.1}Fe_{0.90}O_3$ (*2*), and $BiCo_{0.15}Fe_{0.85}O_3$ (*3*) samples.

magnetization of the samples in comparison with undoped bismuth ferrite. These materials can be promising catalysts for semiconductor oxidation processes, modifying their properties, with the possibility of controlling their parameters using a magnetic field.

The research results were partially obtained on the equipment of The Collective Use Center of Voronezh State University; URL: http://ckp.vsu.ru.

This work was financially supported by the Russian Foundation for Basic Research (Project No. 18-03-00354a).

References

1. J. Wang, J. B. Neaton, H. Zheng, V. Nagarajan, S. B. Ogale, B. Liu, D. Viehland, V. Vaithyanathan, D. G. Schlom, U. V. Waghmare, N. A. Spaldin, K. M. Rabe, M. Wuttig, R. Ramesh, *Science*, 2003, **299**, 1719; DOI: 10.1126/science.1080615.
2. N. A. Spaldin, S. W. Cheong, R. Ramesh, *Phys. Today*, 2010, **63**, 38; DOI: 10.1063/1.3502547.
3. M. Gajek, M. Bibes, S. Fusil, K. Bouzehouane, J. Fontcuberta, A. Barthelemy, A. Fert, *Nature Mater.*, 2007, **6**, 296; DOI: 10.1038/nmat1860.
4. E. Petrova, D. Kotsikau, V. Pankov, *J. Magn. Magnetic Mater.*, 2014, **378**, 429; DOI: 10.1016/j.jmmm.2014.11.076.
5. A. T. Nguyen, Ph. H. Nh Phan, I. Ya. Mittova, M. V. Knurova, V. O. Mittova, *Nanosystems: Phys., Chem., Math.*, 2016, **7**, 459; DOI: 10.17586/2220-8054-2016-7-3-459-463.
6. O. V. Almjasheva, V. V. Gusarov, *Russ. J. Appl. Chem.*, 2016, **89**, 851; DOI: 10.1134/S107042721606001X.
7. M. Fiebig, *J. Phys. D: Appl. Phys.*, 2005, **38**, 123; DOI: 10.1088/0022-3727/38/8/R01.
8. W. Eerenstein, N. D. Mathur, J. F. Scott, *Nature*, 2006, **442**, 759; DOI: 10.1038/nature05023.
9. S. W. Cheong, M. Mostvoy, *Nature Mater.*, 2007, **6**, 13; DOI: 10.1038/nmat1804.
10. R. Ramesh, N. A. Spaldin, *Nature Mater.*, 2007, **6**, 21; DOI: 10.1038/nmat1805.
11. Y. Tokura, *J. Magn. Magn. Mater.*, 2007, **310**, 1145; DOI: 10.1016/j.jmmm.2006.11.198.
12. G. Catalan, J. F. Scott, *Adv. Mater.*, 2009, **21**, 2463; DOI: 10.1002/adma.200802849.
13. Kh. A. Sadykov, I. A. Verbenko, L. A. Reznichenko, A. G. Abubakarov, L. A. Shilkina, O. N. Razumovskaya, S. I. Dudkina, *Konstruktsii iz Kompozitsionnykh Materialov* [*Composite Material Structures*], 2013, **2**, 50 (in Russian).
14. Z. X. Cheng, X. L. Wang, Y. Du, S. X. Dou, *J. Phys. D: Appl. Phys.*, 2010, **43**, 242001; DOI: 10.1088/0022-3727/43/24/242001.
15. G. L. Song, G. J. Ma, J. Su , T. X. Wang, H. Y. Yanga, F. G. Chang, *Ceramics Intern.*, 2014, **40**, 3579; DOI: 10.1016/j.ceramint.2013.09.070.
16. S. K. Pradhan, J. Das, P. P. Rout, V. R. Mohanta, S. K. Das, S. Samantray, D. R.Sahu, J. L. Huang, S. Verma, B. K. Roul, *J. Phys. Chem. Solids*, 2010, **71**, 1557; DOI: 10.1016/j.jpcs.2010.08.001.
17. A. Elídia, I. A. Santos, E. Radovanovic, R. Bonzanini, E. M. Girotto, *J. Braz. Chem. Soc.*, 2008, **19**, 1153; DOI: 10.1590/S0103-50532008000600015.
18. J. Luo, P. A. Maggard, *Adv. Mater.*, 2006, **18**, 514; DOI: 10.1002/adma.200500109.
19. E. V. Tomina, O. V. Ivanova, *Kondensirovannyye Sredy i Mezhfaznyye Granitsy* [*Condensed Media and Phase Boundaries*], 2017, **20**, 148 (in Russian); DOI: 10.17308/kcmf.2018.20/486.
20. C. J. Niepce, D. Stuerga, T. Caillot, J. P. Clerk, A. Granovsky, M. Inoue, N. Perov, G. Pourroy, *IEEE Trans.*, 2002, *Magn.*, **38**, 2622; DOI: 10.1109/TMAG.2002.801963.
21. I. A. Milyaeva, N. S. Perov, V. V. Bessalova, M. V. Berezhnaya, V. O. Mittova, A. T. Nguyen, I. Ya. Mittova, *Nanosystems: Phys., Chem., Math.*, 2018, **9**, 417; DOI: 10.17586/2220-8054-2018-9-3-417-423.
22. A. V. Dmitriev, E. V. Vladimirova, M. V. Kandaurov, A. Yu. Chufarov, D. G. Kellerman, *Fiz. Tverdogo Tela*, 2017, **59**, 2338 [*Russ. Phys. Sol. State* (*Engl. Transl.*), 2017, **59**]; DOI: 10.21883/FTT.2017.12.45228.167.
23. *JCPDC PCPDFWIN: A Windows Retrieval/Display Program for Accessing the ICDD PDF — 2 Data Base*, International Centre for Diffraction Data, 1997.
24. I. Bhat, S. Husain, W. Khan, S. I. Patil, *Mater. Res. Bull.*, 2013, **48**, 4506; DOI: 10.1016/j.materresbull.2013.07.028.
25. F. Dumestre, B. Chaudret, C. Amiens, M. Fromen, M. Casanove, P. Renaud, P. Zurcher, *Angew. Chem., Int. Ed.*, 2002, **41**, 4286; DOI: 10.1002/1521-3773(20021115)41:22<4286:AID-ANIE4286>3.0.CO;2-M.
26. C. Housecroft, E. Constable, *Chemistry: An Integrated Approach*, Prentice Hall, Upper Saddle River, 1997, 1032 pp.
27. Yu. D. Tret´yakov, L. I. Martynenko, A. N. Grigor´ev, A. Yu. Tsivadze, *Neorganicheskaya khimiya. Khimiya elementov: uchebnik dlya studentov vuzov, obuchayushchikhsya po napravleniyu 510500 "Khimiya" i spetsial´nosti 011000 "Khimiya"* [*Inorganic Chemistry. Chemistry of Elements: a Textbook for University Students Studying the Field 510500 "Chemistry" and Specialty 011000 "Chemistry"*], Akademiya, Moscow, 2007, V. **1**, 538 pp.; V. **2**, 670 pp. (in Russian).
28. A. A. Zatyupo, L. A. Bashkirov, I. O. Troyanchuk, G. S. Petrov, A. I. Galyas, L. S. Lobanovskiy, S. V. Trukhanov, I. M. Sirota, *Neorgan. Mater.*, 2013, **49**, 658 [*Inorg. Mater.* (*Engl. Transl.*), 2013, **49**]; DOI: 10.7868/S0002337X13060201.
29. Y. Wei, H. Gui, Z. Zhao, J. Li, Y Liu, S. Xin, X. Li, W. Xie, *AIP Advances*, 2004, **4**, 127134-1; DOI: 10.1063/1.4904811.
30. E. V. Tomina, B. M. Darinskiy, I. Ya. Mittova, V. D. Churkin, N. I. Boykov, O. V. Ivanova, *Neorgan. Mater.*, 2019, **55**, 421 [*Inorg. Mater.* (*Engl. Transl.*), 2019, **55**]; DOI: 10.1134/S0002337X19040158.
31. V. F. Kostryukov, I. Ya. Mittova, B. V. Sladkopevtsev, A. S. Parshina, D. S. Balasheva, *Kondensirovannye sredy i mezhfaznyye granitsy* [*Condensed Media and Phase Boundaries*], 2019, **21**, 215 (in Russian); DOI: 10.17308/kcmf.2019.21/759.
32. E. V. Tomina, I. Y. Mittova, A. A. Samsonov, B. V. Sladkopevtsev, L. S. Zelenina, V. A. Baranova, *Russ. J. Gen. Chem.*, 2017, **87**, 8; DOI: 10.1134/S1070363217010029.

Received September 27, 2019;
accepted January 9, 2020